Appendix

Table of Contents:

Appendix Figure S1

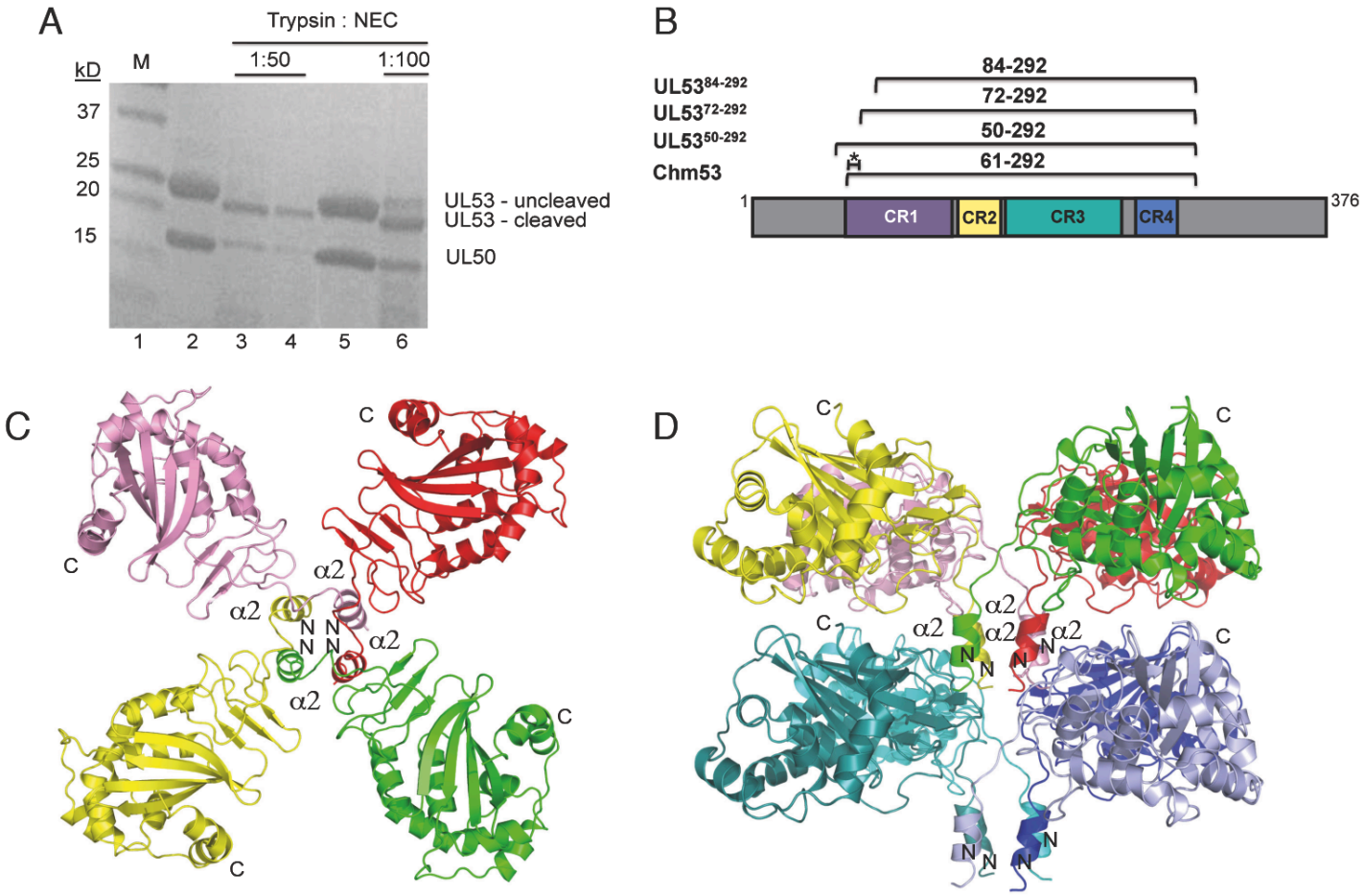

Appendix Figure S2A

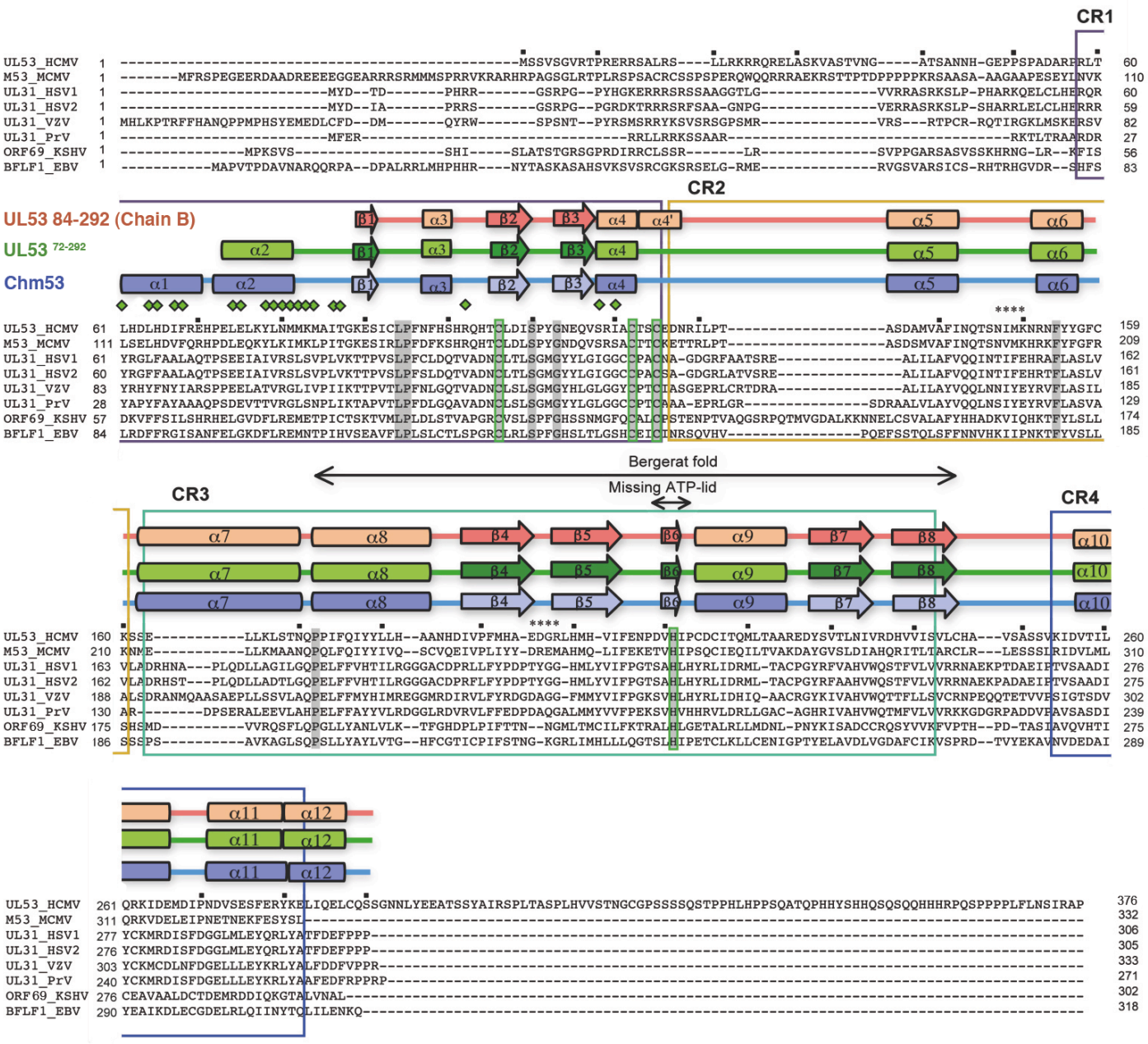

Appendix Figure S2B

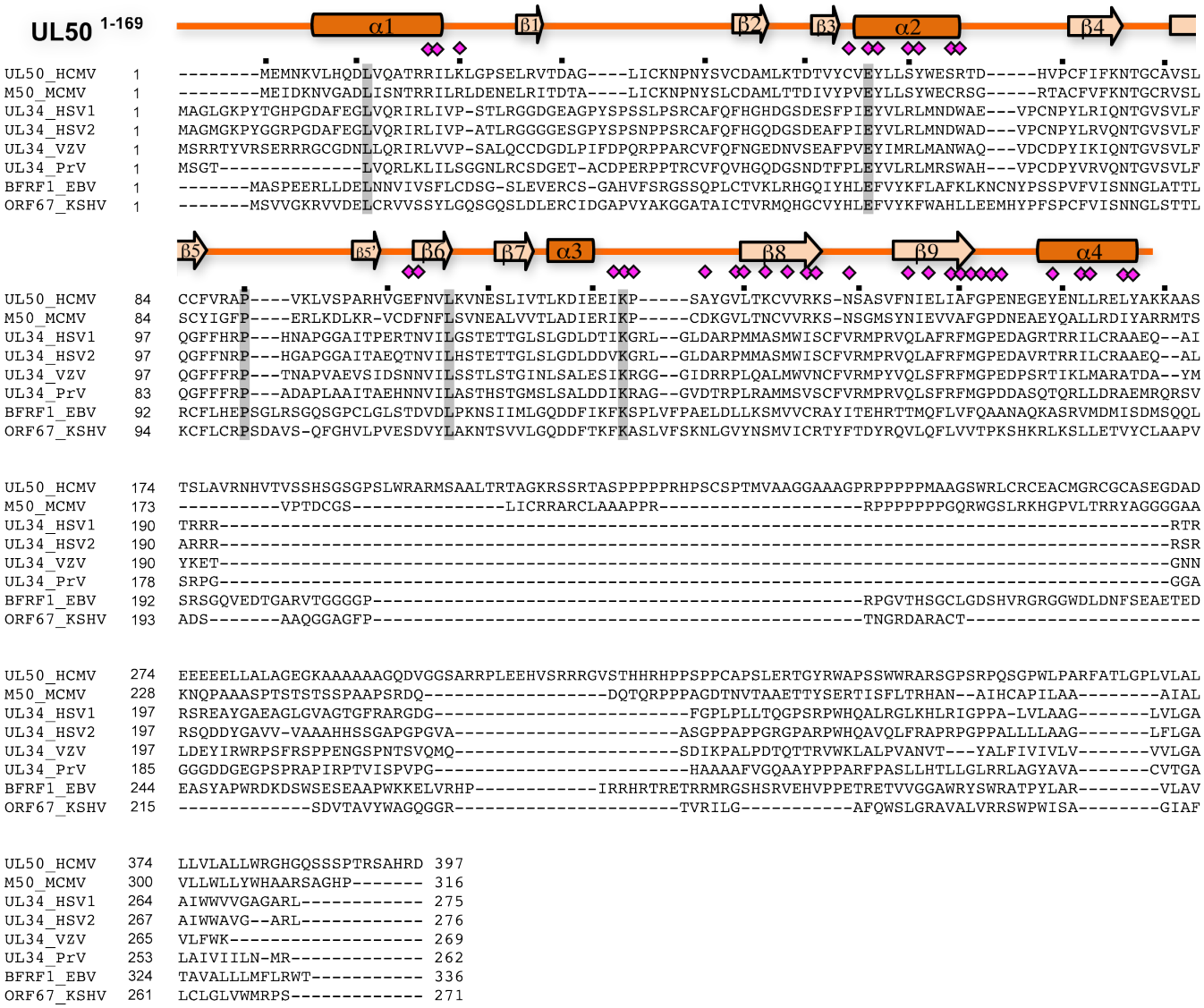

Appendix Figure S3

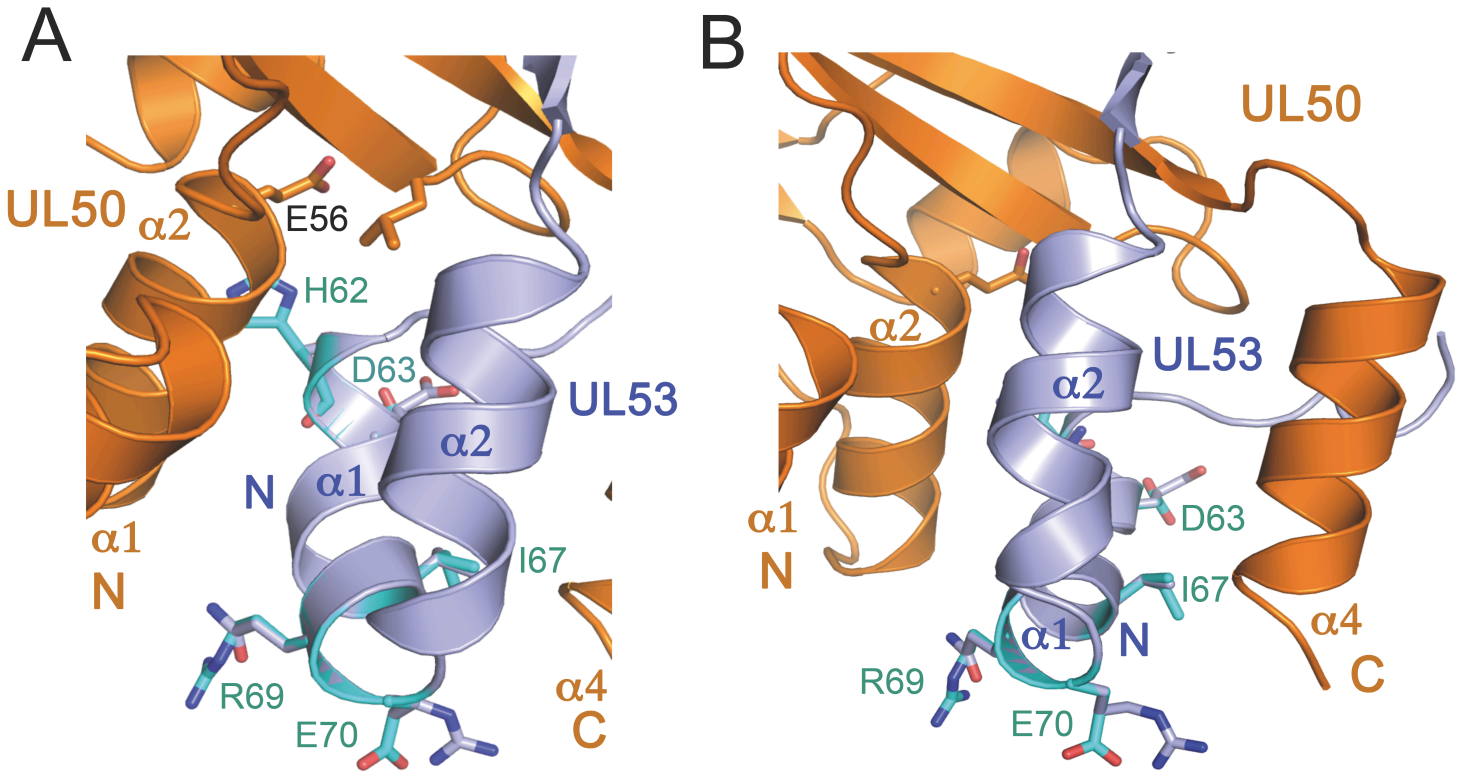

Appendix Figure S4

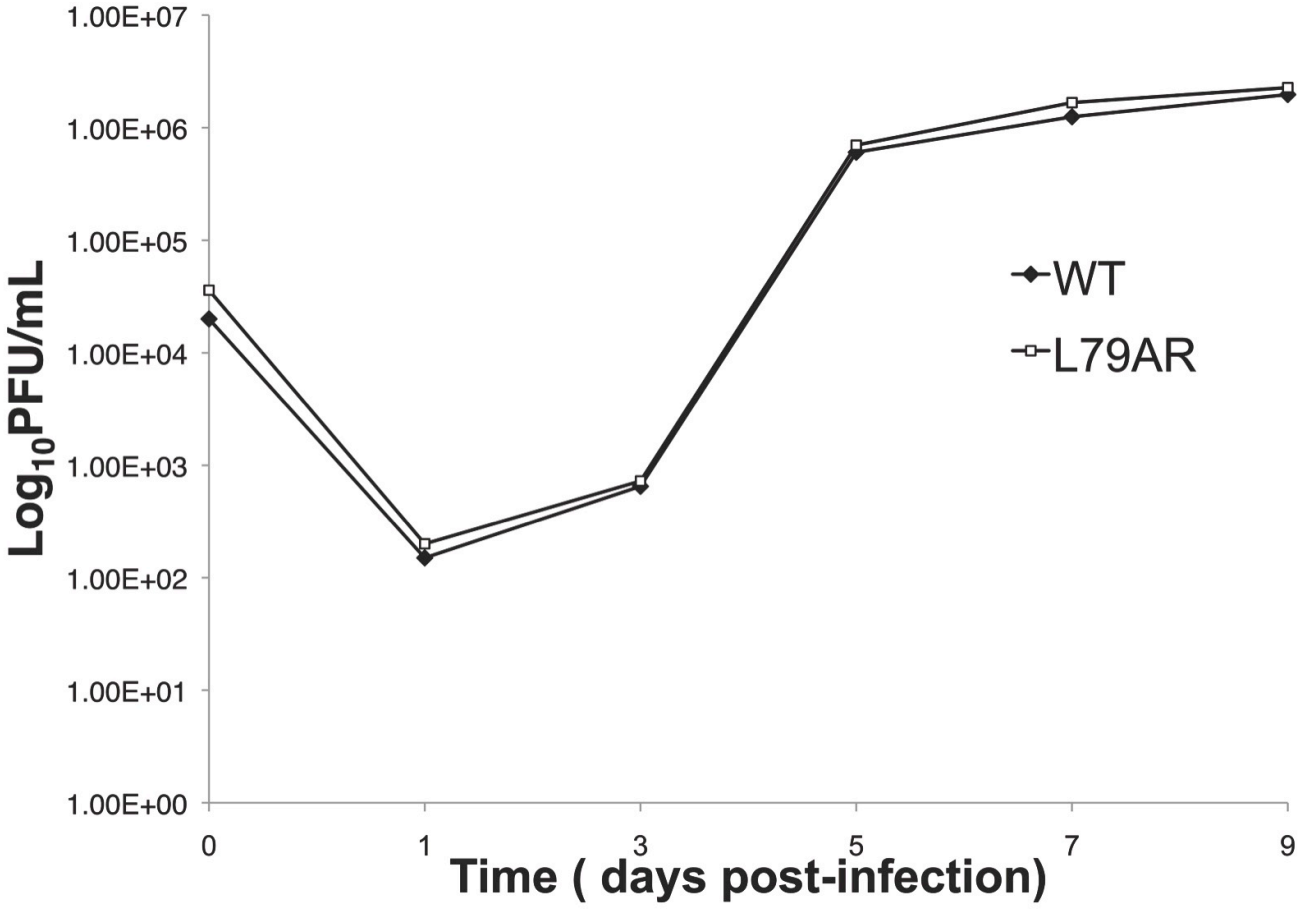

Appendix Figure S5

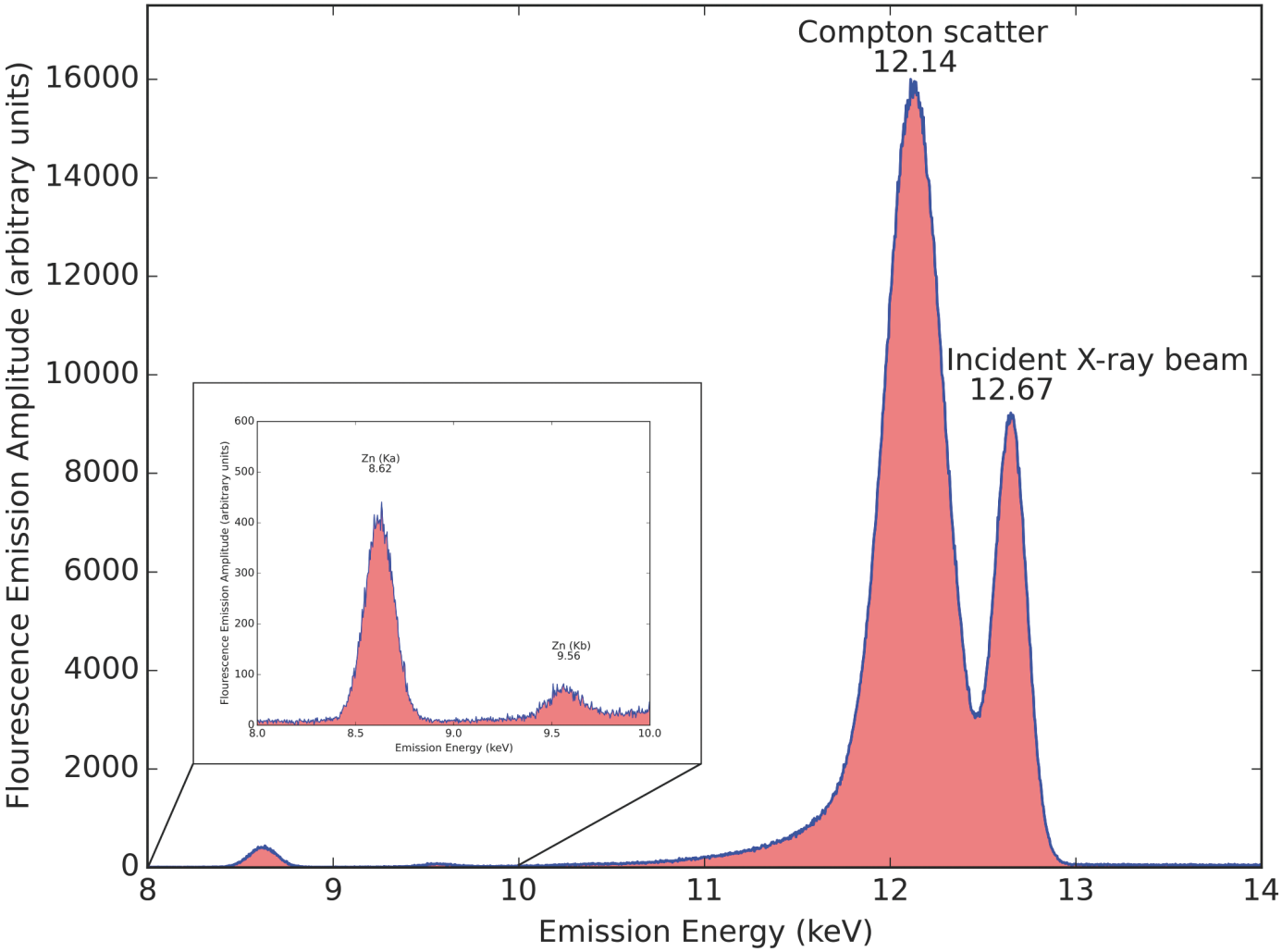

Appendix figure legends

Appendix Figure S1. Crystallization studies on UL53: Construct design and packing of UL53 crystals

A. Trypsin proteolysis studies on purified NEC composed of UL50 encompassing residues 1 to 169 and UL53 encompassing residues 50 to 292. The molecular weight markers are shown in lane 1 with the corresponding weights listed to the left of the Coomassie-stained SDS-PAGE gel. Lanes 2 and 5 have uncut NEC for comparison with trypsin treated NEC. The NEC samples were treated with two different ratios of trypsin to NEC – 1:50, a sample of which is run in lane 3 and 4 at two different dilutions, and 1:100, a sample of which is run in lane 6. In lane 6, the upper most band corresponds to uncleaved UL53 while the second band corresponds to a cleaved UL53 fragment. The bottom band is UL50 and was uncleaved. At a higher trypsin to NEC ratio (1:50), UL53 is fully cut, while UL50 remains uncleaved.

B. Schematic representation of the UL53 constructs used for crystallization studies. The boundaries of the residues used in each construct are shown above the respective brackets. The conserved regions (CR) across the herpesvirus families are color-coded. In Chm53, which was used to form the NEC, the boundaries correspond to residues 61 to 292 in UL53 except that five residues at the N-terminus were substituted by the corresponding residues in the mouse homolog (M53). These substitutions resulted in greatly improved diffraction of the NEC crystals.

C. Top view of each monomer of $UL53^{72-292}$ clustered around the four-fold rotation axis in the P4 space group through the N-terminus α2 helix.

D. Crystal packing of $UL53^{72-292}$ showing the alternating layers of the cluster of α2 helices with the rest of the UL53 body.

Appendix Figure S2. Structure-based sequence alignment of UL50 and UL53 against selected homologs with the interaction interface mapped.

A. Alignment of the UL53 (UniProtKB identifier: P16794) sequence with homologs from α (HSV-1 (P10215), HSV-2 (P89454), and varicella zoster virus (VZV (P09283))), β (MCMV (A8E1D1)), and γ (Kaposi's sarcoma herpesvirus (ORF69_KSHV (F5H982) and Epstein-Barr virus (BFLF1_EBV (P0CK47))) herpesvirus sub-families. Identical residues are highlighted in gray and the three cysteine residues and one histidine (C_3H) residue of the zinc finger are boxed in green. The secondary structure elements of $UL53^{84-292}$ (chain B, shades of red) are shown with that of $UL53^{72-292}$ (shades of green) and Chm53 (shades of purple). The CRs among the herpesviruses are shown in boxes following the same color scheme as in Fig 1D. The Bergerat fold in CR3 of UL53 and the segment that replaces an ATP-binding loop region (ATP-lid) in UL53 is labeled on the alignment. Residues that interact with UL50 are indicated by the green diamonds above the UL53 sequence. Residues that mediate crystal contacts between UL53 (both as a monomer and as part of the NEC) in the different crystal forms obtained are labeled with an asterisk (*). The identity between the full-length sequence of UL53 with M53 and HSV-1

UL31 is 41.3% and 15.4% respectively, while that between residues encompassing only the CRs (from residues 56 to 282 in UL53 with the homologous residues in M53 and HSV-1 UL31) is 55.1% and 16.0% respectively.

B. Alignment of the UL50 (P16791) sequence with homologs from the α (HSV-1 (P10218), HSV-2 (P89457) and VZV (P09280)), β (MCMV (A8E1C8)), and γ (ORF76_KSHV (F5HA27) and BFRF1_EBV (P03185)) herpesvirus sub-families. The secondary structure elements of $UL50^{1-169}$ (orange) are shown above the sequence. Residues that interact with UL53 are indicated by the pink diamonds above the UL50 sequence. The identity between the full-length sequence of UL50 with M50 and HSV-1 UL34 is 43.4% and 17.8% respectively, while that between residues encompassing only the conserved N-terminal region (from residues 1 to 173 in UL53 with the homologous residues in M53 and HSV-1 UL31) is 60.5% and 17.3% respectively.

Appendix Figure S3. Modeling UL53 residues substituted in Chm53 onto the NEC (Chm53:UL50)

A. Close-up view of the UL53 helices against the UL50 core. The original residues in the UL53 sequence (cyan) are modeled onto the Chm53 structure and overlaid with the M50 residues (purple) used in the construct. Five UL53 residues (H62, D63, I67, R69, E70) were substituted for their M50 homologs (S62, E63, V67, Q69, R70). The orientation of the structure is the same as that in Fig 5D.

B. Close-up view of the UL53 helices with the α4 of UL50. The original residues in the UL53 sequence (cyan) are modeled onto the Chm53 structure and overlaid with the M50 residues (purple) used in the construct. Five UL53 residues (H62, D63, I67, R69, E70) were substituted for their M50 homologs (S62, E63, V67, Q69, R70). Of these five residues, only V67 is involved in heterodimer contacts. The orientation of the structure is the same as that in Fig 5E.

Appendix Figure S4. Replication kinetics of the L79 rescued derivative

The replication kinetics of the rescued derivative of the UL53 mutant L79A, L79AR (□) was compared with WT BADGFP virus (◆) after inoculation at a multiplicity of infection (MOI) of 0.1 pfu per cell of 10^5 human foreskin fibroblast (HFF) cells per well in 24-well plates. For each data point, the supernatants from two wells were pooled on the indicated day post-infection, and titers were calculated by averaging plaque counts from duplicate titrations. Counts from duplicate titrations differed by less than a factor of two for all data points. Error bars are not shown.

Appendix Figure S5. Validation of zinc in UL53

Energy-dispersive X-ray spectroscopy (EDS) spectrum of frozen protein solution. The K-α1 and K-β1 emission line peaks for Zn are shown in the inset zoom region between 8 to 10 keV. The large peaks at 12.14 keV and 12.67 keV are generated by Compton scattered X-rays and the incident X-ray beam, respectively.

Appendix Table S1. Summary of the effects of mutations on UL53 and UL50 at the interaction interface.

UL53	K_d (μM)	Co-localization with UL50 in co-transfection assays	Growth phenotype of virus containing mutations	Reference
WT	0.29		Viable	Sam et. al., 2009, and this study
L64A	4.1	nd[b]	Viable	Sam et. al., 2009, and this study
F68A	9.5	nd[b]	Viable	Sam et. al., 2009, and this study
L74A	0.63	nd[b]	nd[b]	Sam et. al., 2009
E75A	No binding[a]	None	Non-viable	Sam et. al., 2009, and this study
L79A	No binding[a]	None	Non-viable	Sam et. al., 2009, and this study
M82A	10-50	None	Non-viable	Sam et. al., 2009, and this study
UL50	K_d (μM)	Co-localization with UL53 in co-transfection assays	Growth phenotype of virus containing mutations	Reference
WT	0.29		Viable	Leigh *et. al.,* 2015
E56A	30-90	None	Non-viable	Leigh *et. al.,* 2015
Y57A	No binding[a]	nd[b]	nd[b]	Leigh *et. al.,* 2015
L130A	7.9	None	Non-viable	Leigh *et. al.,* 2015
Δ153	No binding[a]	nd[b]	nd[b]	This study
Y159,L162-AA	nd[b]	None	Non-viable	This study
$_{159}$YENL$_{162}$-AAAA	nd[b]	None	Non-viable	This study

[a] Binding was undetected either by isothermal titration calorimetry or by column chromatography

[b] nd; not determined

Appendix Table S2. Summary of primers for UL50 and UL53 constructs in protein expression vectors and mutant plasmids for crystallization and gel filtration studies

For transfer of UL50 and UL53 genes from Inteine plasmids (Sam, 2009) into a pGEX6p and pET15b vector respectively		
Plasmid	**Primer**	**Sequence**
Int-UL50 (residues 1-169)	Int-UL50_Fw	CAGAATGCTGGT**CATATG**GAGATGAACAAGGTTCTC
	Int-UL50_Rv	CTGTACGCCAAGTAA**GAATTC**TCGACGTCGTTGGCG
Int-UL53 (residues 50-292)	Int-UL53_Fw	CAGAATGCTGGT**CATATG**TCGCCGGCCGAC
	Int-UL53_Rv	CAGTCCAGCGGCTAA**GAATTC**CTCGAGCCC
UL53 mutants		
Plasmid	**Primer**	**Sequence**
61-292	start61_Fw	*CAG GGG CCC* CTG GGA TCC CTG CAC GAC CTG CAC
72-292	start72_Fw	*CAG GGG CCC* CTG GGA TCC CCC GAA CTG GAG CTC
84-292	start84_Fw	*G GGG CCC* CTG GGA TCC ATG GCC ATC ACG GGC
Chm53	Chm53_1a_Fw	CTG GGA TCC ATG CTG AAG CTG AGC GAG CTG CAC GAC GTC TTC CAG CGC CAC CCC GAA CTG GAG
UL50 mutant		
Plasmid	**Primer**	**Sequence**
1-152	end152_Fw	GAG CTC ATC GCC TTC GGA **TAA** GCC GCG TCG AC

The restriction sites (NdeI and EcoRI) are shown in bold. In italics is the sequence for precision protease, while the gene sequences are underlined.

Appendix Table S3. (A). Summary of mutant constructs in the HCMV BAC or pcDNA plasmid background. (B). Primer sequences for changes introduced into the HCMV AD160 BAC of UL53 and UL50

A. Construct	Genetic Background	Source	Change Introduced
UL53 sequence			
E75A	pBADGFP	Sharma *et. al.* 2014 (1)	Mutation of residue E75 to alanine
L79A	pBADGFP	Sharma *et. al.* 2014 (1)	Mutation of residue L79 to alanine
M82A	pBADGFP	Sharma *et. al.* 2014 (1)	Mutation of residue M82 to alanine
E75AR	E75A pBADGFP	This study	Restored the WT UL53 coding sequence
L79AR	L79A pBADGFP	This study	Restored the WT UL53 coding sequence
M82AR	M82A pBADGFP	This study	Restored the WT UL53 coding sequence
Chm53	53-F pBADGFP	Sharma *et. al.* 2014 (1)	Introduced M53 helix 1 sequence corresponding to the construct used in crystallization
C106S	53-F pBADGFP	Sharma *et. al.* 2014 (1)	Mutation of residue C106 to serine
H211A	pBADGFP	This study	Mutation of residue H211 to alanine
C106SR	C106S 53-F pBADGFP	This study	Restored the WT UL53 coding sequence
H211AR	H211A53-F pBADGFP	This study	Restored the WT UL53 coding sequence
Plasmid constructs			
L79A	pcDNA FLAG-UL53	Sam *et. al.*, 2009 (2)	Mutation of residue L79 to alanine
C122S	pcDNA FLAG-UL53	Sam *et. al.*, 2009 (2)	Mutation of residue C122 to serine
C125S	pcDNA FLAG-UL53	Sam *et. al.*, 2009 (2)	Mutation of residue C125 to serine
H211A	pcDNA FLAG-UL53	Sam *et. al.*, 2009 (2)	Mutation of residue H211 to alanine
SI-AA	pcDNA FLAG-UL53	Sam *et. al.*, 2009 (2)	Mutation of residues S118 and I120 to alanine
UL50 sequence			
$2A/_{159}AENA_{162/}$	pBADGFP	Sharma *et. al.* 2014 (1)	Mutation of residues Y159 and L162 to alanine
$4A/_{159}AAA_{162/}$	pBADGFP	Sharma *et. al.* 2014 (1)	Mutation of residues Y159, E160, N161 and L162 to alanine
Plasmid constructs			
$2A/_{159}AENA_{162/}$	pcDNA HA-UL50	Sam *et. al.*, 2009 (2)	Mutation of residues Y159 and L162 to alanine
$4A/_{159}AAAA_{162/}$	pcDNA HA-UL50	Sam *et. al.*, 2009 (2)	Mutation of residues Y159, E160, N161 and L162 to alanine

B.

UL53 BADGFP constructs		
Construct	**Primer**	**Sequence**
E75A	E75A Fw	CGACCTGCACGACATCTTCCGCGAGCACCCCGAACTGGCCCTCAAGTACCTTAA CATGATTAGGGATAACAGGGTAATCG
	E75A Rv	TGCCCGTGATGGCCATCTTCATCATGTTAAGGTACTTGAGGGCCAGTTCGGGGT GCTCGCGGAGCCAGTGTTACAACCAATTAACC
L79A	L79A Fw	CGACATCTTCCGCGAGCACCCCGAACTGGAGCTCAAGTACGCCAACATGATGAA GATGGCCTAGGGATAACAGGGTAATCGATTT
	L79A Rv	AGATGGACTCTTTGCCCGTGATGGCCATCTTCATCATGTTGGCGTACTTGAGCT CCAGTTCGCCAGTGTTACAACCAATTAACC
M82A	M82A Fw	CGAGCACCCCGAACTGGAGCTCAAGTACCTTAACATGGCCAAGATGGCCATCAC GGGCAATAGGGATAACAGGGTAATCG
	M82A Rv	GTAAGCAGATGGACTCTTTGCCCGTGATGGCCATCTTGGCCATGTTAAGGTACT TGAGCTGCCAGTGTTACAACCAATTAACC
E75AR	E75AR Fw	CGACCTGCACGACATCTTCCGCGAGCACCCCGAACTGGAGCTCAAGTACCTTAA CATGATTAGGGATAACAGGGTAATCG
	E75AR Rv	TGCCCGTGATGGCCATCTTCATCATGTTAAGGTACTTGAGCTCCAGTTCGGGGT GCTCGCGGAGCCAGTGTTACAACCAATTAACC
L79AR	L79AR Fw	CGACATCTTCCGCGAGCACCCCGAACTGGAGCTCAAGTACCTTAACATGATGAA GATGGCCTAGGGATAACAGGGTAATCGATTT
	L79AR Rv	AGATGGACTCTTTGCCCGTGATGGCCATCTTCATCATGTTAAGGTACTTGAGCTC CAGTTCGCCAGTGTTACAACCAATTAACC
M82AR	M82AR Fw	CGAGCACCCCGAACTGGAGCTCAAGTACCTTAACATGATGAAGATGGCCATCAC GGGCAATAGGGATAACAGGGTAATCG
	M82AR Rv	GTAAGCAGATGGACTCTTTGCCCGTGATGGCCATCTTCATCATGTTAAGGTACTT GAGCTGCCAGTGTTACAACCAATTAACC
Chm53	CHM53Fw	GGCGAACCGCCGTCGCCGGCCGACGCGCGCCCGCGCCTGAAGCTGAGCGAG CTGCACGACGTCTTCCAGCGCCACCCCGAACTGGAGCTCAAGTAGGGATAACA GGGTAAT
	CHM53 Rv	CTTCATCATGTTAAGGTACTTGAGCTCCAGTTCGGGGTGGCGCTGGAAGACGTC GTGCAGCTCGCTCAGCTTCAGGCGCGGGCGCGCGTCG GCCAGTGTTACAACCAATTAACC
C106S	C106S Fw	TACCCTTCAATTTCCACTCGCACCGGCAGCACACCTCCCTCGACATCTCGCCGT ACGGCATAGGGATAACAGGGTAATCG
	C106S Rv	GCGAGACCTGCTCGTTGCCGTACGGCGAGATGTCGAGGGAGGTGTGCTGCCG GTGCGAGTGGCCAGTGTTACAACCAATTAACC
C106SR	C106SR Fw	TACCCTTCAATTTCCACTCGCACCGGCAGCACACCTGCCTCGACATCTCGCCGT ACGGCATAGGGATAACAGGGTAATCG
	C106SR Rv	GCGAGACCTGCTCGTTGCCGTACGGCGAGATGTCGAGGCAGGTGTGCTGCCG GTGCGAGTGGCCAGTGTTACAACCAATTAACC
H211A	H211A Fw	GTTGCACATGCACGTCATCTTCGAAAACCCCGACGTGGCCATCCCCTGCGACTG CATCACTAGGGATAACAGGGTAATCG
	H211A Rv	GCGCCGCCGTGAGCATCTGCGTGATGCAGTCGCAGGGGATGGCCACGTCGGG GTTTTCGAGCCAGTGTTACAACCAATTAACC
H211AR	H211AR Fw	GTTGCACATGCACGTCATCTTCGAAAACCCCGACGTGCACATCCCCTGCGACTG CATCACTAGGGATAACAGGGTAATCG
	H211AR Rv	GCGCCGCCGTGAGCATCTGCGTGATGCAGTCGCAGGGGATGTGCACGTCGGG GTTTTCGAGCCAGTGTTACAACCAATTAACC

UL50 BADGFP constructs		
Construct	**Primer**	**Sequence**
2A/159AENA162/	2A Fw	TCGAGCTCATCGCCTTCGGACCCGAAAACGAGGGCGAGGCAGAGAATGC TCTGCGCGAGCTGTACGCCTAGGGATAACAGGGTAATCG
	2A Rv	ACGTCGACGCGGCTTTCTTGGCGTACAGCTCGCGCAGAGCATTCTCTGCC TCGCCCTCGTTTTCGGGGCCAGTGTTACAACCAATTAAC
4A/159AAA162/	2A Fw	TCGAGCTCATCGCCTTCGGACCCGAAAACGAGGGCGAGGCAGCCGCGGC TCTGCGCGAGCTGTACGCCTAGGGATAACAGGGTAATCG
	2A Rv	ACGTCGACGCGGCTTTCTTGGCGTACAGCTCGCGCAGAGCCGCGGCTGC CTCGCCCTCGTTTTCGGGGCCAGTGTTACAACCAATTAAC
2AR	2A Fw	TCGAGCTCATCGCCTTCGGACCCGAAAACGAGGGCGAGTACGAGAATCTG CTGCGCGAGCTGTACGCCTAGGGATAACAGGGTAATCG
	2A Rv	ACGTCGACGCGGCTTTCTTGGCGTACAGCTCGCGCAGCAGATTCTCGTAC TCGCCCTCGTTTTCGGGGCCAGTGTTACAACCAATTAAC

1. Sharma, M., J. P. Kamil, M. Coughlin, N. I. Reim, and D. M. Coen. 2014. Human cytomegalovirus UL50 and UL53 recruit viral protein kinase UL97, not protein kinase C, for disruption of nuclear lamina and nuclear egress in infected cells. J Virol 88:249-62.

2. Sam, M. D., B. T. Evans, D. M. Coen, and J. M. Hogle. 2009. Biochemical, biophysical, and mutational analyses of subunit interactions of the human cytomegalovirus nuclear egress complex. J. Virol. 83:2996-3006.

3. Tischer, B. K., G. A. Smith, and N. Osterrieder. 2010. En passant mutagenesis: a two step markerless red recombination system. Methods Mol Biol 634:421-30.

4. Tischer, B. K., J. von Einem, B. Kaufer, and N. Osterrieder. 2006. Two-step red-mediated recombination for versatile high-efficiency markerless DNA manipulation in Escherichia coli. Biotechniques 40:191-7.

Appendix Supplementary Methods

Trypsin proteolysis of the NEC

Trypsin proteolysis was conducted using the Proti-Ace kit from Hampton Research following the manufacturer's instructuctions. Briefly, 170 mM of NEC was incubated in either a 1:50 or 1:100 ratio of trypsin (0.01 mg/mL) to NEC at 37° for 1 hour. The reaction was quenched by the addition of 4X SDS-PAGE sample buffer to each sample and the samples were run on an SDS polyacrylamide gel. The products from the digest were cut from the gel and the sequences analyzed using mass spectrometry by the Taplin Mass Spectrometry Facility at Harvard Medical School.

Viruses

HCMV replication following infection at a multiplicity of infection of 0.1 was assessed as described previously (Sharma et al, 2014). Titration was done by infecting $1x10^5$ HFF cells per well (in a 24-well plate) with serial dilutions of harvested virus samples for 1 h, following which the inocula were replaced with media containing methylcellulose. After 14 days, the monolayers were stained with crystal violet and plaques were counted using a dissecting microscope. Titers represent average values from duplicate samples.